Linear 1-D Analysis of Oscillations in Hall Thrusters

by

Reid Noguchi*, Manuel Martinez-Sanchez** and Eduardo Ahedo†

Abstract

A one-dimensional, linear perturbation model was formulated to aid in the analysis of the low-frequency axial oscillation instabilities observed during the operation of Stationary Plasma Thrusters. The first six solutions of this 1st order perturbation model were determined by scanning the complex frequency plane and were addressed in this study. Of these modes, two notable patterns of behavior were found and discussed. The first group of modes had waves which translated through the thruster, with a fundamental harmonic of 49.7 kHz. The second group, having a fundamental harmonic of 74.2 kHz, exhibited a sloshing type of behavior and was found to have several characteristics of an ionization (predator-prey) type cycle. All modes were found to be highly damped.

1. *Introduction*

Many experiments have evidenced the existence of strong longitudinal oscillations in Hall thrusters. The simplest manifestation of these oscillations is a modulation of the anode current, typically, in the 20-30 kHz range for thrusters in the 1 kW power range. The overall voltage may also show some ripple, but this is strongly inhibited by the large parallel capacitance typically used in the external circuit. These oscillations can be fairly deep, up to full 0-100% current modulation, but they are sometimes much weaker or almost absent. In other experiments it has been noticed that oscillations do not occur until the ceramic insulator has accumulated some visible sputter deposition in regions not directly under the hottest plasma (i.e., until a few tens of hours of operation). Since surface state may control Te (via secondary emission), this suggests some coupling to ionization dynamics.

A very direct visualization of these oscillations was reported by Darnon et al [1.2], showing a total absence of azimuthal structure, a regular brightening and dimming of the ionization region, and an associated pulsation of the plasma beam downstream of it. Up to three harmonics of the basic frequency were also observed. More recent experimental work by Pagnon et al [3] shows further details of these oscillations' in particular, by ensemble-averaging of a number of time traces following a sharp occasional fluctuation, it was shown that the ensuing oscillations were in all cases damped within a few cycles. This suggests a logical separation between the triggering events, which remain obscure, and the response of the plasma to these events. It is this response that we study in this work. Previous attempts at understanding the nature of these oscillations; have typically focussed on the dynamics of the ionization process. Thus, Kim et al [4] describes in qualitiative terms a type of relaxation oscillation in which the periodic re-kindling of the plasma occurs when fresh neutrals arrive to replenish those ejected in the previous cycle.

The detailed 2-D, particle- in-Cell simulations of Fife [5,6] have shown oscillations as well, and an analysis of these numerical results [6] appears to support a local ionization cycle of the "predator-prey" type, with electrons acting as predator species and neutrals as the prey. On the other hand, data by Fife [7] on and SPT-70 appear to be insensitive to flow and voltage, and strongly resemble acoustic type oscillations.

In this paper, we extend our ongoing work on one-dimensional fluid modeling of Hall thrusters [8] by allowing transient small disturbances. The new linearized equations allow both, acoustics and ionization to occur and interact. At this time, only situations for which the thruster exit is choked are included in the model, although an extension to cases with an internal sonic passage is straightforward.

2. *Formulation*

Other than the inclusion of time-dependent effects, our basic formulation is that of Ref. [8]: a one-dimensional 3-fluid model (electrons, ions, neutrals), with ionization kinetics determined by the local electron temperature. The governing

* Graduate Student, MIT, Cambridge, MA (USA). Currently at Lockheed Martin.
** Professor of Aeronautics/Astronautics, MIT. Cambridge, MA (USA).
† Polytechnical University of Madrid (Spain).

equations are collected together in Table 1. Wall effects and electron heat conduction were neglected.

2.1 *Steady State*

The steady-state solutions of these equations were discussed in [8], where it was shown that the proper inlet condition for ions is that they are falling back into the anode sheath at their ion-sonic speed $c_i = \sqrt{\frac{5}{3}kT_e/m_i}$. We selected one of the solutions with a choked exit (i.e., local ion sonic speed at exit) at $T_e = 1.4E_i/k$, and with an arbitrarily selected electron temperature just beyond the inlet sheath of $0.1E_i/k$ (E_i=ionization energy). This steady solution is shown in Fig. 1. Densities are normalized by $\dot{m}/\left(A\sqrt{m_i E_i}\right)$, velocities by $\sqrt{E_i/m_i}$, and lengths by an arbitrary quantity $\ell^* = 10mm$. Xenon gas is assumed. This basic solution shows the characteristic narrow ionization zone near the sonic exit, with a sharp T_e maximum just ahead of it. The ion velocity is very low (and mostly negative) in the diffusion layer, and accelerates rapidly in the ionization region.

2.2 *Linearization about the Steady State*

The next step is to linearize the equations of Table 1 about the steady state solution, in the general form

$$f(x,t) = \tilde{f}(x) + \sum_{modes,j} \mathrm{Re}\left(\hat{f}_j(x) e^{i\omega_j t} \right) \qquad (1)$$

where $\hat{f}(x)$ represents the (normalized steady-state solution for quantity f, and $\hat{f}_j(x)$ is the modal shape of the jth mode, which oscillates with a complex frequency ω_j. Frequencies with a positive imaginary part indicate damped modes, while any negative imaginary part would signal instability. The frequencies are to be obtained as eigenvalues of the system of linear homogeneous differential equations, with appropriate homogenous boundary conditions.

The linearized equations can be obtained by straightforward algebraic procedures, but are omitted here due to space limitations. A full account can be found in Ref. [9].

The steady-state governing equations, when solved for the separate spatial derivatives, have right-hand-sides of the form $F/\left(1-\tilde{M}_i^2\right)$, where F depends on all state variables, and $\tilde{M}_i = v_i/c_i$. Choked solutions, as assumed there, will have infinite slopes (with integrable singularities of type $\frac{const.}{\sqrt{|x-x_{sonic}|}}$ at the inlet and exit points. Alternatively, smooth sonic passage is possible if F=0 when $\tilde{M}_1 = 1$ (see Ref. [8]). In the process of linearization, additional possibilities for singular behavior arise. It is shown in Ref. [9] that all perturbation spatial derivatives can be obtained from one of them, say $\frac{d\hat{\phi}}{dx}$, and that this derivative has the form

$$\left(1-\tilde{M}_i^2\right)\frac{d\hat{\phi}}{dx} = \frac{\hat{G}}{1-\tilde{M}_i^2} + \hat{H} \qquad (2)$$

where $\hat{G}$ and $\hat{H}$ are non-singular linear functions of all the perturbation variables, with spatially varying coefficients (derived from the zero-th order solution). Focussing now on the type of steady-state solution used here, in which all derivatives are singular lat sonic points, we see that we can tolerate $\hat{H} \neq 0$ in Eq. (2), which will make the perturbation variable singular of the same order, but not $\hat{G}$=o, because perturbations would then be more singular than basic variables, which invalidates the linearization assumption $|\hat{f}/\tilde{f}| << 1$. This leads us to the condition $\hat{G}$=o at any point where $|\tilde{M}_i| = 1$, and it is found that this implies

$$\hat{M}_i = o \text{ when } |\tilde{M}_i| = 1 \qquad (3)$$

i.e., the sonic (singular) points remain sonic even during the transients. Physically, convective derivatives dominate at these points over temporal variations (at any finite frequency) A similar, but slightly more involved argument can be used to obtain conditions at a smooth sonic passage (in that case $\frac{\hat{G}}{1-\tilde{M}_i^2}$ is automatically

finite, and one must then impose $\hat{H} + \hat{G}/(1 - \tilde{M}_i^2) = o$ when $|\tilde{M}| = 1$.

The special conditions $\hat{M}_i = o$ at both inlet and exit constitute two of the five required homogenous boundary conditions for the perturbation equations. A third condition is the invariance of the inlet mass flow rate (the injectors are assumed to remain choked). A fourth condition is the equality of the potential perturbations at inlet and exit; if the exit were at cathode potential, this would be justified by the presence of a large parallel capacitor, but since we terminate the calculation at the thruster exit plane, before supersonic expansion, this must be regarded as a provisional device, pending the incorporation of an appropriate plume model. Finally, we impose zero fluctuation of electron temperature at the exit; if the potential fluctuations are small at that point, those of T_e should also be small, since electrons gain energy from the potential difference cathode-exit plane.

2.3 Numerical Implementation

The homogeneous problem outlined in the previous section has non-trivial solutions only if the complex frequency ω takes one of a (presumably infinite) sequence of specific values. In principle, then, one can guess ω, then integrate the differential equations, satisfying all but one of the homogeneous boundary conditions; the error in this remaining condition can be used as an index to locate the correct values in the complex ω map. We used a variation of this general procedure to account for the fact that some of the conditions are known upstream and some downstream: for each condition which is not prescribed at the inlet, a basic solution is computed, where one unknown is given an initial value of 1, and the other unknown quantities are made zero. The complete solution is a linear superposition of these basic solutions, and imposing at the exit the conditions which apply there yields a set of linear homogeneous equations for the combination constants. Forcing compatibility of these equations yields the nonlinear equation for ω. This equation was solved by a direct search procedure in the complex ω plane.

3. Results

3.1 Frequencies

The lowest six ω eigenvalues for our problem are shown in Table 2, both, normalized by $\frac{1}{\ell^*}\sqrt{\frac{E_i}{m_i}}$, and in physical units. The imaginary parts are all positive, and are ≈0.3-0.5 of the real parts, showing substantial damping for all modes found. No unstable condition was identified. The real parts show frequencies starting at 47.9 kHz. These are of the order reported for thrusters in which the internal channel has a length of the order of the 1.5cm assumed here (see Fig. 1). In addition to the damped oscillatory modes, there is also a pure subsidence mode (ω_R=o, ω_I>o), which would be observable only as a decay of some imposed disturbance.

3.2 Character of the Modes

For each of the identified complex frequencies, the modal shapes $\hat{n}_e(x)$, $\hat{v}_i(x), \hat{\phi}(x), etc$, are of interest. These are complex quantities, and the amplitude and phase scales are chosen such that the normalized current perturbation $\hat{j}/\tilde{j}$ is unity. Alternatively, the physical perturbations can also be constructed for each variable in each mode, (i.e. the second part of Eq. (1)

Ref. [9] contains complete records of these quantities for all six modes found. Here we will only present some of the more informative results.

It was found that (aside from the subsidence mode), there were two different types of behavior: Modes 2 (47.9kHz), 4 (102kHz) and 5 (122 kHz) are forward-travelling waves, whereas modes 3 (74.2 kHz) and 6 (162 kHz) resemble standing-wave patterns. This is illustrated by the space-time contour plots of electron number density perturbation in modes 2 and 3 (Figs. 2,3). In particular, Mode 3 (Fig. 3) shows one modal point at $x/\ell^* = 0.85$, where n_e does not fluctuate; similar calculation for v_i show that the fluctuation is generally negative to the right of this mode, and positive to the left, indicating a kind of "sloshing" motion. By contrast, Mode 2 (Fig. 2) shows a clear travelling wave pattern, with no nodes.

Modes 3 and 6 differ from the others in one other important respect. As shown in Figures 4 and 5

and in Table 3, all modes show substantial ionization rate fluctuations in the same region where steady state ionization happens. In the travelling modes (2,4,5) the densities of neutrals and plasma

Mode no.	Real part of Normalized Frequency	Phase($\hat{n}_e$)- -Phase ($\hat{n}_n$)
2	1.28	-9°
3	1.98	+58°
4	2.72	0°
5	3.25	-23°
6	4.33	+95°
Predator-Prey	2.5	90°

Table 3: Approximate phase lead of $\hat{n}_e$ over $\hat{n}_n$ in the ionization layer, for modes 2-6. For reference, the "Predator-Prey" model results are also shown

fluctuate roughly in phase with each other, but in modes 3 and 6 (the standing wave modes), the electron density fluctuations lead those of the neutrals by something like 90°. This is what one would expect in a "predator-prey" type of ionization oscillation [6].

A simplified derivation of this model (follows, for reference: assume ionization occurs in a layer of thickness L_i, into which only neutrals flow at velocity v_n, and out of which only ions flow, at velocity v_i. Then

$$\frac{dn_e}{dt} - \frac{v_i}{L} n_e = \alpha n_e n_n \qquad (4)$$

$$\frac{dn_n}{dt} + \frac{v_n}{L} n = -\alpha n_e n_n \qquad (5)$$

where $\alpha(T_e)$ is the ionization rate constant. To zero'th order (steady state), it follows that $\frac{\tilde{v}_i}{L} = \alpha \tilde{n}_n$ and $\frac{\tilde{v}_n}{L} = \alpha \tilde{n}_e$. To first perturbation order, assuming $\alpha(T_e)$ and the velocities do not vary, and using the zero'th order results,

$$\frac{dn_e'}{dT} = \alpha \tilde{n}_e n_n' \qquad (6)$$

$$\frac{dn_n'}{dt} = \alpha \tilde{n}_n n_e' \qquad (7)$$

so that $\frac{d^2 n_e'}{dt^2} + \left(\alpha^2 \tilde{n}_e \tilde{n}_n\right) n_e' = o$ (8)

with a similar equation for n_n'. Equation (6) shows that n_e' leads n_n' by 90°, and equation (8) gives an oscillation frequency

$$\omega = \alpha \sqrt{\tilde{n}_e \tilde{n}_n} \qquad (9)$$

Fig. 6 shows the steady-state solution (same as Fig. 1, but for the narrow ionization region only). The quantity R_{ion} shown in the last panel is $\alpha \tilde{n}_e \tilde{n}_n$, so that Eq. (9) is also

$$\omega = \frac{R_{ion}}{\sqrt{\tilde{n}_e \tilde{n}_i}} \qquad (10)$$

Using averages between $x/\ell^* = 1.43$ and 1.47, this yields a predator-prey normalized frequency $\omega \cong 2.5$; this is close to the computed. Mode 2 frequency, (Table 3).

The model leading to Eq. (9) assumes that the ionization dynamics involves mainly n_e and n_n fluctuations, with $\alpha(T_e)$ remaining constant. This seems at first sight inaccurate, because T_e does fluctuate in the ionization layer (see Figs. 4a and 5a). However, as Table 4 shows, these fluctuations are indeed secondary compared to those of n_e and n_n:

Sloshing Mode no.	$\frac{\hat{n}_e}{\tilde{n}_e}$	$\frac{\hat{n}_n}{\tilde{n}_n}$	$\frac{\hat{T}_e}{\tilde{T}_e}$	$\frac{\hat{\alpha}}{\tilde{\alpha}}$
3	0.3	1	0.07	0.1
6	0.4	1	0.07	0.1

Table 4: Relative magnitude of terms in Ionization rate perturbation

In contrast with these "sloshing modes", where ionization dynamics appears dominant, the other modes are seen to be mainly acoustic in nature. The densities n_e, n_n merely fluctuate together as the wave's compression and rarefaction phases pass by. The existence of these two different families of modes, one where the frequency seems to be controlled by wavenumber and speed of sound (acoustics), the other by ionization kinetics, raises the question of what may happen when conditions are adjusted such that two modes, one from each family, coincide in frequency. This might be forced, for example by surface conditions changes that may affect the electron temperature (mainly then affecting the

ionization frequencies). This remains a topic for future work, however.

4. *Discussion*

Our model appears to capture and analyze adequately two types of small amplitude oscillations (acoustic and ionization modes) in Hall thrusters. All modes are found to be well damped, in agreement with the experimental data on the evolution of individual excitation events [3] . The model does not capture, however, the occasional large amplitude excursions which trigger these oscillations in the experiments. This could be due to unmodelled physical mechanisms, or could simply reflect the linearization, which would miss large-amplitude nonlinear effects. A recent paper by Garrigues et al [10] has used two different 1-D, time-dependent models to simulate the transients in SPT thrusters, and both show a higher frequency nonlinear mode in which a soliton-like spike of high field intensity and ionization rate originates at the anode and then races downstream. Similar effects were also found earlier in our two-dimensional PIC simulations [7] , and took the form of an apparent ionization burst near the anode, which created a localized potential hump; the subsequent high field on the downstream side of this region created new ionization there, and led to a rapid forward propagation. This was not reported because it appeared very sensitive to details of the near-anode model, but, in retrospect, the phenomenon may be real, and may play a role in the generation of the triggering events. What remains unexplained, however, is the intermittent nature of these events (both models in Ref. [1] predict regular, high frequency "soliton" sequences).

The linear results shown here all refer to sonic (singular exit) channels, with a very stiff sonic condition on the oscillations. The recently completed work of Ahedo (unpublished) to generate and study steady-state solutions with smooth sonic passage and supersonic exit should lead to corresponding extensions of this unsteady analysis. As noted before, we also hope to perform parametric variations in search of the possibly new phenomena that would result from coincidence of the freqencies of an ionization and an acoustic mode.

5. *Conclusions*

A linearized transient analysis has been developed for a one-dimensional Hall thruster channel. Special conditions at the sonic point were derived, which, for a choked exit, amount to zero ion Mach number perturbation at that point. Two families of damped modes were identified, one mainly acoustic, with forward propagation, the other mainly ionization-related with standing wave patterns.

References

1. F. Darnon, M. Lyszyk and A. Bouchoule, "Optical Investigation of Plasma Oscillations of SPT Thrusters". Paper AIAA 97-3051, 33rd Joint Propulsion Conf., Seattle, WA, July 1997.
2. F. Darnon, C. Kadlec-Phlippe, A. Bouchoule and M. Lyszyk, "Dynamic Plasma and Plume Behavior in SPT Plumes". Paper AIAA 98-3644, 34th Joint Propulsion Conf., Cleveland, OH, July 1998.
3. Pagnon, D., Darnon F, et al, "Time-Resolved Characterization of the Plasma and Plume of a SPT Thruster", Paper AIAA 99-2428, 35th Joint Propulsion Conf., Los Angeles, June 1999.
4. Garvyushin, V.M, Kim, V. et al, "Study of the Effect of Magnetic Field Variation, Channel Geometry Change and its Walls Contamination upon the SPT Performance". Paper AIAA 94-2858, 30th Joint Propulsion Conf., Indianapolis, June 1994.
5. Fife, J.M and Martinez-Sanchez, M, "Two-Dimensional PIC Modeling of Hall Thrusters, Paper IEPC-95-240, 24th IEPC Conf., Moscow, Sep. 1995.
6. Fife, J.M., Martinez-Sanchez, M. and Szabo, J., "A Numerical Study of Low Frequency Discharge Oscillations in Hall Thrusters". Paper AIAA 97-3052, 33rd Joint Propulsion Conf., Seattle, WA, July 1997.
7. Fife, J.M., Hybrid PIC Modeling and Electrostatic Probe Survey of Hall Thrusters, Ph.D. Thesis, MIT, 1998.
8. Ahedo, E. and Martinez-Sanchez, M., "One-Dimensional Plasma Structure in Hall Thrusters". Paper AIAA 98-8788, 34th Joint Propulsion Conf., Cleveland, OH, July 1998.
9. Noguchi, R., "Linear 1-D Analysis of Oscillation Instabilities in Stationary Plasma Thrusters". Masters Thesis, MIT, Dept. of Aeronautics/Astronautics, May 1999.

10. Garrigues, L., Heron, A., Adam, J.C. and Boeuf, J.P., "Comparisons between Hybrid and PIC Models of a Stationary Plasma Thruster". Paper AIAA 98-2297, 35th Joint Propulsion Conf., Los Angeles, CA, June 1999.

Plasma Dynamic Equations	Principle of Equation
$\frac{\partial n_e}{\partial t} + \frac{\partial}{\partial x}(v_i n_e) = n_e \upsilon_{ion}$	conservation of ions n_e = electron number density v_i = ion velocity υ_{ion} = ionization frequency per electron
$\frac{\partial n_e}{\partial t} + \frac{\partial}{\partial x}(v_e n_e) = n_e \upsilon_{ion}$	conservation of electrons v_e = electron velocity
$\frac{\partial n_n}{\partial t} + \frac{\partial}{\partial x}(v_n n_n) = -n_e \upsilon_{ion}$	conservation of neutrals n_n = neutral number density v_n = neutral velocity
$m_i\left(\frac{\partial v_i}{\partial t} + v_i\frac{\partial v_i}{\partial x}\right) = -q\frac{\partial \phi}{\partial x} - \upsilon_{ion} m_i (v_i - v_n)$	conservation of momentum for ions m_i = ion mass ϕ = electric potential
$0 = q\frac{\partial \phi}{\partial x} - \frac{1}{n_e}\frac{\partial}{\partial x}(n_e k T_e) - \upsilon_H m_i v_e$	conservation of momentum for electrons k = Boltzman constant T_e = electron temperature $\frac{m_i}{m_e}\upsilon_H$ = effective collision frequency for axial diffusion
$\frac{\partial}{\partial t}\left(\frac{3}{2}n_e k T_e\right) + \frac{\partial}{\partial x}\left(\frac{5}{2}n_e k T_e v_e\right) = n_e\left(q v_e \frac{\partial \phi}{\partial x} - \upsilon_{ion} E_i'\right)$	conservation of energy q = electric charge E_i' = effective ionization energy
$\upsilon_{ion} = \sigma_0 n_n \sqrt{\frac{8kT_e}{\pi m_e}}\left(1 + 2\frac{kT_e}{eE_i}\right)e^{-\frac{eE_i}{kT_e}}$	ionization frequency σ_0 = ionization cross section m_e = electron mass
$\frac{m_i}{m_e}\upsilon_H = \frac{\left(\alpha_B \omega_C \frac{m_i}{m_e}\right)^2}{n_n \sigma_{en}\sqrt{\frac{8kT_e}{\pi m_e}} + \alpha_B{}^2 \omega_C \frac{m_i}{m_e}}$	effective collision frequency for axial diffusion α_B = Bohm diffusion coefficient ω_C = characteristic cyclotron frequency σ_{en} = electron-neutral collision cross section

Table 1: Simplified Plasma Dynamic Equations

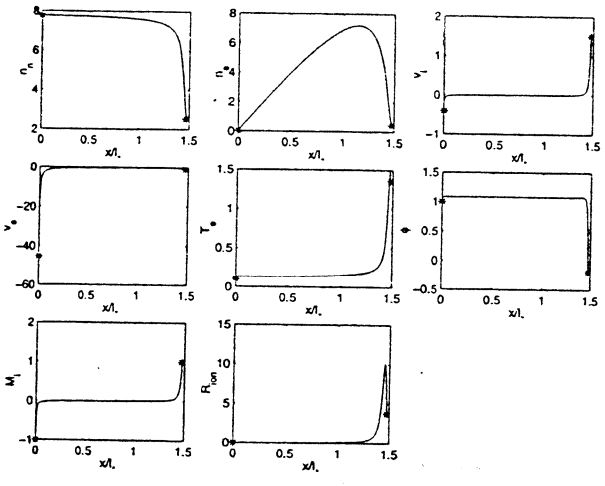

Fig 1: 0th Order State Variables

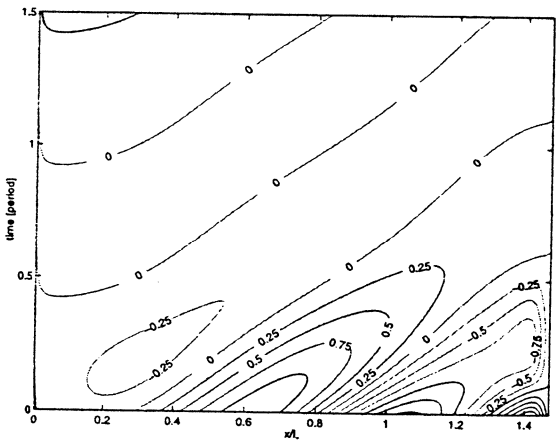

Fig. 2: Propagation of Electron Number Density Perturbation for f_r=47.9kHz ($\tilde{\omega}$=1.279+0.651i)

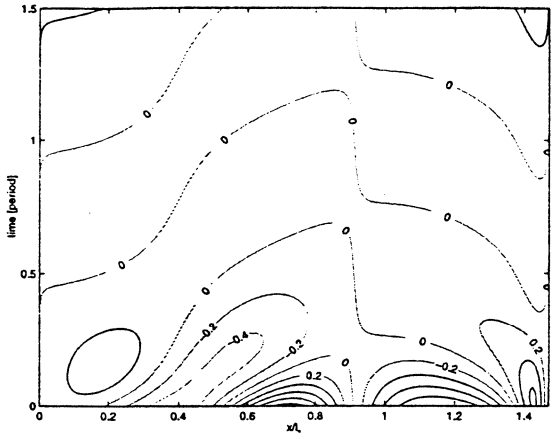

Fig 3: Propagation of Electron Number Density Perturbation for fr=74.2kHz
($\tilde{\omega}$=1.982+1.473I)

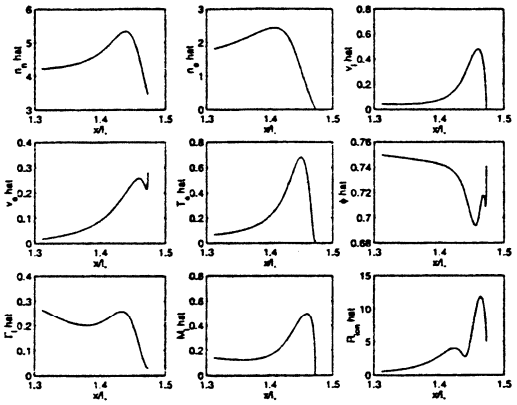

Fig. 4a: Perturbation Magnitudes in Ionization Layer for f_r=47.9kHz
($\tilde{\omega}$=1.279+0.651I)

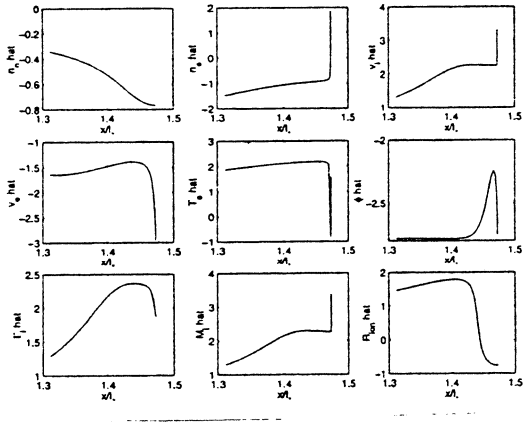

Fig. 4b: Perturbation Phases in Ionization Layer for f_r=47.999kHz
($\tilde{\omega}$=1.279+0.651i)

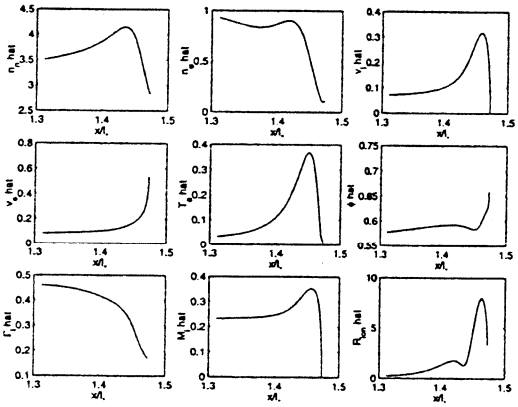

Fig. 5a: Perturbation Magnitudes in Ionization Layer for f_r=74.2kHz
($\tilde{\omega}$=1.982+1.473i)

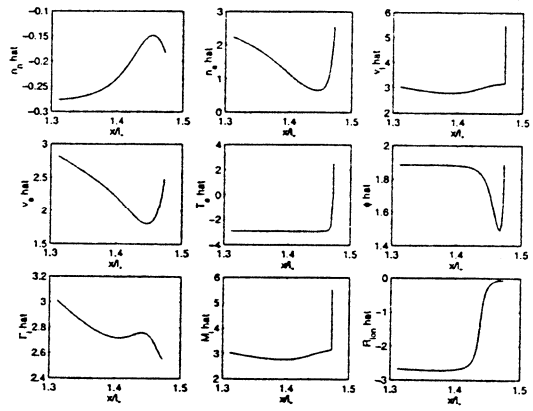

Fig. 5b: Perturbation Phases in Ionization Layer for f_r=74.2kHz
($\tilde{\omega}$=1.982+1.473i)

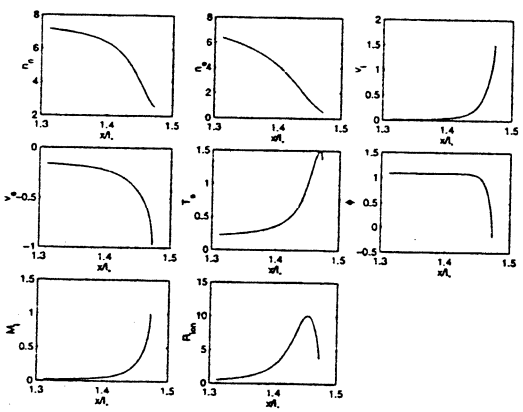

Fig. 6: 0th Order State Variables in the Ionization Layer